ADVANCED MATERIALS

DOI: 10.1002/adma.200602781

Acid-Functionalized Mesostructured Aluminosilica for Hydrophilic Proton Conduction Membranes**

By *George L. Athens*, *Yair Ein-Eli*, and *Bradley F. Chmelka**

New proton exchange membrane (PEM) materials with high proton conductivities at elevated temperatures (ca. >150 °C) offer the promise of improving PEM fuel cell operation. Higher operating temperatures would provide several benefits including: (i) improved resistance to carbon monoxide poisoning of the platinum (Pt) electrocatalyst at the anode,[1–3] (ii) reduced need for feed-stream heat and humidity management,[4,5] and (iii) faster reaction kinetics at both electrodes.[6,7] Reforming of natural gas and other hydrocarbons provides a hydrogen feed stream that typically contains ~10 % CO, with subsequent water-gas shift and preferential CO oxidation reactions able to reduce the concentration down to ~10 ppm CO.[5,8] However, carbon monoxide levels as low as 10 ppm can interfere with H_2 adsorption on the dispersed Pt catalyst at the anode, detrimentally affecting the performance of PEM fuel cells operating at temperatures below 100 °C.[3] At higher operating temperatures, it has been shown that H_2 adsorption on the Pt electrocatalyst becomes competitive with CO adsorption, with the result that PEM fuel cells can stably function at higher CO levels, e.g., 100 ppm at temperatures ≥150 °C.[9] Operating temperatures above 140 °C are therefore expected to improve significantly the performance of proton exchange membrane fuel cells that use hydrogen generated from hydrocarbon fuel sources.

Currently, most PEM fuel cells use polymeric or polymer-inorganic composite membrane materials that must be chemically stable, provide structural support, and have low permeability to diffusing reactant and product species, in addition to conducting protons. Widely used perfluorosulfonic-acid polymers, such as Nafion®, provide and balance these properties under conditions in which they remain hydrated. For example, Nafion 117® exhibits typical conductivity values of ~0.1 S cm^{-1} under fully hydrated conditions at room temperature.[10] However, as their extent of hydration decreases, such as occurs under conditions of low humidity or elevated temperatures, their proton conductivities also decrease.[11,12] At temperatures above 150 °C, where CO poisoning of the Pt catalyst becomes less troublesome,[9] water loss of perfluorosulfonic-acid-polymer PEMs is a major limitation, as their strongly hydration-dependent proton conductivities decrease to below 10^{-3} S cm^{-1}.[13,14]

Consequently, there has been extensive interest in the development of alternative proton exchange membrane materials that retain high proton conductivities at elevated temperatures near 150 °C. The majority of new membrane materials are based on continuous *organic* polymer matrices with sulfonic-acid,[15,16] aromatic,[17,18] and/or acid-base functional groups[19,20] or containing inorganic particle additives, such zeolites or silica.[21,22] Each of these materials balances various membrane property attributes differently.[23] For example, sulfonated aromatic polymers are characterized by good thermal and chemical properties, while possessing proton conductivities between 10^{-3}–10^{-1} S cm^{-1} at temperatures up to 140 °C.[18,24] The higher conductivity values are obtained for aromatic polymer membranes possessing high degrees of sulfonation, although this tends to be accompanied by poorer mechanical properties at high temperatures, due to increased membrane swelling.[23] Acid-base polymer membranes, such as H_3PO_4-doped polybenzimidazole (PBI), exhibit proton conductivity values up to 0.13 S cm^{-1} at 160 °C.[25] However, PBI-H_3PO_4 membranes similarly attain high proton conductivities at high acid-doping levels and high temperatures, conditions under which the membranes also exhibit swelling and poor mechanical properties.[23,24] By comparison, inorganic-organic composite membranes, such as those containing hydrophilic zeolite, silica, or titania particles introduced into Nafion® or other polymers tend to retain more water, with modest improvements in their proton conductivities.[22,26–28] Likewise, improved water retention and proton conductivity have been obtained through the incorporation of inorganic particles into other proton exchange membrane materials.[24] Alternatively, porous inorganic particles have been functionalized by proton-conducting species[29–33] or filled with proton-conducting polymers.[34] Extensive efforts to develop new organic-polymer-based PEMs are summarized in several com-

[*] Prof. B. F. Chmelka, Dr. G. L. Athens
Department of Chemical Engineering, University of California
Santa Barbara, CA 93106 (USA)
E-mail: bradc@engineering.ucsb.edu
Prof. Y. Ein-Eli
Department of Materials Engineering
Technion—Israel Institute of Technology
32000 Technion City, Haifa (Israel)

[**] We thank Dr. Y. S. Kim and Dr. P. Zelenay for helpful discussions. This work was supported in part by the MURI program of the USARL and USARO under grant no. DAAD 19-03-1-0121. G.L.A. was supported by the IGERT program of the U.S. National Science Foundation under award no. DGE-9987618. The work made use of the central facilities of the UCSB Materials Research Laboratory supported by the MRSEC Program of the National Science Foundation under award No. DMR 05-20415. We thank BASF for the donation of the F127 triblock copolymer species. B.F.C. was a 2006 Joseph Meyerhoff Visiting Professor at the Weizmann Institute of Science, Rehovot, Israel. Supporting Information is available online from Wiley InterScience or from the authors.

prehensive recent reviews[23,24,35,36] to which the reader is referred for more detailed property comparisons. While these approaches have generally increased bulk hydrophilicity of the respective materials, they have led to relatively moderate improvements in bulk proton conductivity at temperatures above 100 °C, largely because the continuous polymeric host matrices present the same hydration-dependent conduction barriers as in the non-composite materials.

Here, we present the synthesis and characterization of novel acid-functionalized, mesostructured aluminosilica films for use as proton exchange membranes at temperatures above 150 °C. These new materials combine several attributes that are not available in previously reported membranes based on polymeric, inorganic, or composite solids. In particular, they use block-copolymer-templated silica that can be processed into films with robust mesostructured channels that can be functionalized to produce desirable water-retention and proton conduction properties. Such materials maintain interconnected channels through the membrane that are independent of the extent of hydration. When functionalized with hydrophilic and strong acid moieties, the channels furthermore promote enhanced proton conduction through the membrane, notably under conditions (temperature, humidity) that resist CO-poisoning of fuel cell electrocatalysts.

Acid-functionalized mesostructured aluminosilicas exploit useful properties from their various components that are not achievable collectively from the individual materials. For example, nanoporous aluminosilicate zeolites are known to be highly hydrophilic, though are challenging to prepare as crack-free membranes and are moreover difficult to functionalize.[37] By comparison, block-copolymer-templated mesoporous silica can be synthesized with three-dimensionally interconnected channels (e.g., with a cubic $Im\bar{3}m$ space group structure) that can furthermore be easily processed into robust films for membrane applications. Following calcination or solvent extraction to remove the structure-directing block-copolymer species, post-synthesis grafting of aluminosilica moieties onto the interior mesopore walls introduces both hydrophilic and acidic surface properties.[38,39] While mesoporous silica or aluminosilica alone have relatively poor proton conduction properties,[40] incorporation of strong acid moieties, such as perfluorosulfonic acid species, onto their interior mesopore surfaces and channels results in films with high and stable proton conductivities, even at temperatures above 150 °C.

The preparation of a heterogeneous membrane material that combines high mesoscale ordering, crack-free inorganic film integrity, high hydrophilicity, and high proton conductivity, however, is exceedingly difficult to achieve in a single processing step. This is because the physicochemical interactions that account for the distributions of key species and moieties within such materials often (and indeed usually) cannot be simultaneously controlled to meet all property criteria under a single set of synthesis conditions. Nevertheless, such properties can be readily obtained in combination by 'staged processing' of mesostructured materials, whereby multiple functionalities and properties are incorporated and optimized separately in sequence. Doing so provides substantially greater versatility for selecting materials synthesis and processing conditions to achieve the combination of properties desired. Such versatility has been key to the development of multiply functionalized mesostructured silica membranes, the preparation of which include the following principal steps: formation of a block-copolymer-directed cubic silica film, removal of the block-copolymer to produce mesoporosity, sequential grafting of hydrolyzed alumina and perfluorosulfonic-acid species onto interior mesopore surfaces, and lastly pore-backfilling with triflic or other acid species. As described below, each of these steps introduce important properties that are infeasible or not possible to incorporate in a single or combined processing steps.

Mesostructured silica films were first prepared by the evaporation-induced self-assembly method,[41–43] using amphi-philic block-copolymer species as structure-directing and film forming agents. This was achieved by dip-coating a precursor solution of poly(ethyleneoxide)-*b*-poly(propyleneoxide)-*b*-poly(ethyleneoxide) triblock copolymer species, e.g., Pluronic™ F127 ($EO_{106}PO_{70}EO_{106}$) in the presence of a hydrolyzed silica species under acidic conditions[44] onto a polished silicon substrate at room temperature. As the substrate was withdrawn from the precursor solution, volatile solvent components evaporated from the deposited film, thereby promoting self-assembly of the triblock copolymer species, along with co-assembly and subsequent formation of a densely cross-linked silica network.[43] Film thickness was controlled by varying the ethanol concentration, and thus the viscosity, of the dip-coating solution, and/or by adjusting the dip-coating rate, with the process being complete in ca. 1 min. Alternatively, free-standing mesostructured silica films were cast from an identical precursor solution in an open vessel, from which volatile components were allowed to evaporate over the period of about 1 week. The structure-directing triblock copolymer species were subsequently removed by either calcination or solvent extraction (see Experimental Sec.) to introduce mesoporosity into the films. The scanning electron micrograph (SEM) in Figure 1a shows a representative supported calcined film that is crack-free with smooth and uniform 190 nm thickness that could be adjusted between 100–500 nm by controlling the processing conditions. Similarly, the SEM image in Figure 1b, shows a representative free-standing solvent-extracted film with a thickness of (62 ± 5) μm, which could be varied from 30–150 μm while maintaining film integrity.

Mesostructural ordering in the silica films is generated by the amphiphilic block copolymer species, according to the solution composition and conditions selected. Here, the relative concentrations of the F127® ($EO_{106}PO_{70}EO_{106}$) triblock copolymer, solvents (water and ethanol), and hydrolyzed silica species were combined under ambient conditions[45] to yield an $Im\bar{3}m$ cubic-structured silica network with three-dimensionally interconnected pores. Ordering at such mesoscopic length scales was characterized by transmission electron microscopy (TEM), small-angle X-ray diffraction (SAXS), and nitrogen adsorption isotherms. Representative TEM images are shown in the inset images in Figure 1a and b for the sup-

ADVANCED MATERIALS

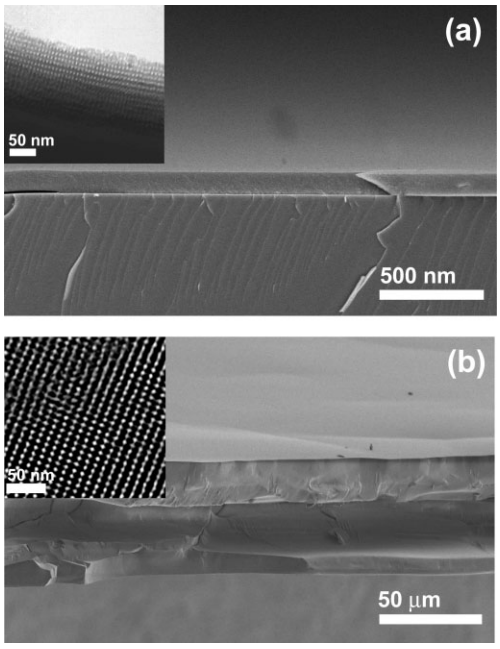

Figure 1. Electron microscopy images of mesoporous silica films with cubic ($Im\bar{3}m$) structures. a) SEM and TEM (inset) micrographs showing a tilted cross-sectional view and cubic pore ordering, respectively, for a 190 nm-thick silica film prepared by dip-coating on a polished silicon wafer. b) SEM and TEM (inset) micrographs showing similar features for a 62 μm-thick free-standing film.

ported calcined dip-coated silica films and free-standing solvent-extracted silica films, both of which display high extents of local cubic mesostructural ordering. SAXS results in Figure 2 acquired for the as-synthesized and solvent-extracted free-standing silica films confirm their highly ordered $Im\bar{3}m$ cubic mesostructures. The SAXS pattern of the as-synthesized silica-F127 film (Fig. 2a) shows three Bragg reflections, whose d-spacings at 15.1 nm, 11.2 nm, and 9.3 nm can be indexed to the (110), (200), and (211) reflections, respectively, of the body-centered-cubic space group $Im\bar{3}m$,[44] with a unit cell parameter $a = 21.4$ nm. After removal of the structure-directing triblock copolymer species, the silica network contracts, consistent with the (110) and (200) reflections appearing at higher 2θ values and broadening of the (211) reflection (Fig. 2b). Mesostructural ordering in the solvent-extracted silica films is retained, with a d_{110} spacing of 11.7 nm measured for the narrow (*110*) reflection, corresponding to a 23 % contraction of the unit cell to $a = 16.5$ nm. Similar SAXS results (Supporting Information Fig. S1) were obtained for the as-synthesized and calcined supported silica films. These results are separately consistent with nitrogen sorption data: a Barrett–Joyner–Halenda (BJH) analysis of the adsorption branch of the nitrogen isotherm (Supporting Information Fig. S2) establishes a mesopore size distribution sharply peaked at a mean diameter of (8.2 ± 0.4) nm, and ~3 nm-thick silica pore walls in the free-standing solvent-extracted silica film. These results, in combination, establish the existence of a well-ordered 3D-interconnected network of mesopores within the silica films.

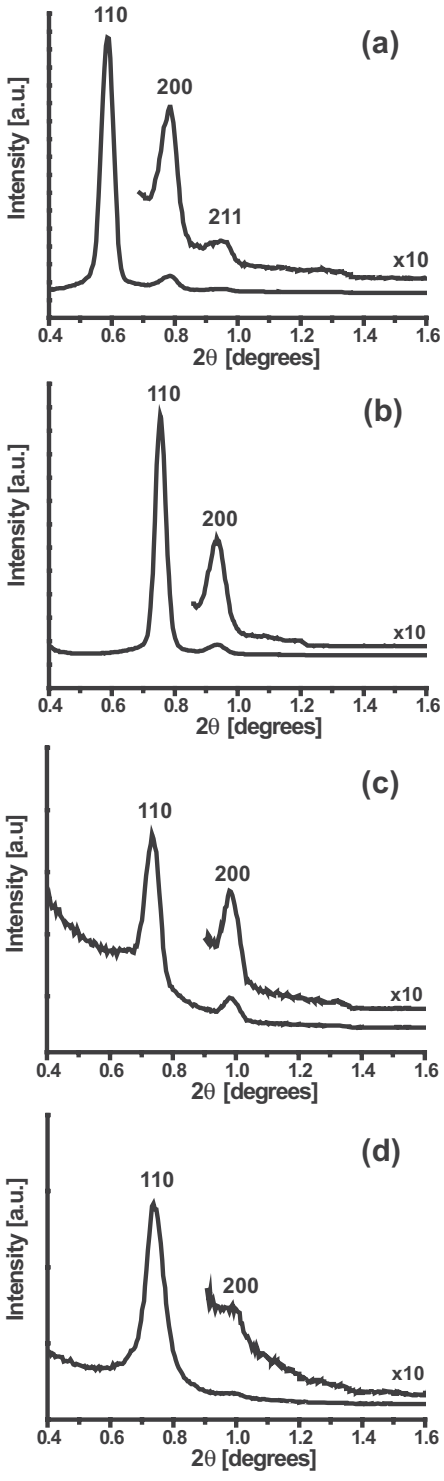

Figure 2. Small-angle X-ray scattering patterns of a free-standing mesostructured silica film after each of the following sequence of treatments: a) as-synthesized, (b) solvent-extracted, (c) aluminosilica-grafted (Si/Al = 15), and d) perfluorosulfonic-acid- and aluminosilica-grafted mesoporous silica films. The diffraction patterns are indexed to the body-centered-cubic ($Im\bar{3}m$) structure. The 1D plots are azimuthal integrals of 2D scattering patterns obtained by transmission mode XRD with the beam oriented perpendicular to the plane of the films. b) Corresponds to the same film shown in Figure 1b.

Though silica itself is only modestly hydrophilic and is not strongly acidic, the large pores, high internal surface area, and facile grafting procedures allow the internal pore surfaces to be functionalized with more hydrophilic and/or more acidic moieties to enhance their water-retention and proton-conduction properties. Siliceous frameworks are comprised of Si^{IV} pecies that are four-coordinated to oxygen atoms and so are charge neutral and relatively hydrophobic. By comparison, grafting four-coordinate Al^{III} sites onto the interior mesopore surfaces (as aluminosilica species) introduces anionic charges into the framework, each site of which requires a charge-compensating cation, such as H^+, to preserve overall charge neutrality. Such ions render these surface sites highly hydrophilic, with the bulk hydrophilicity of a film depending on the extent of surface aluminosilica functionalization.

Incorporation of aluminosilica moieties in powders or films has typically been accomplished via "direct syntheses," in which hydrolyzed sources of silica and alumina are mixed together in a precursor solution, after which the components co-condense.[46] While this approach works well for the preparation of mesoporous aluminosilica powders, co-condensation of silica and alumina precursors during evaporation-induced self-assembly of mesostructured films under acidic conditions leads to products with limited extents of four-coordinate Al incorporation.[46] In addition, the aluminosilica moieties are distributed throughout the pore walls, as opposed to only on the surface sites. For modest to high Al contents, e.g., Si/Al molar ratios of ≤ 50, the mesostructural ordering of such co-condensed films has been shown to decrease drastically with increasing Al concentration,[47] leading in extreme cases to macroscopic phase separation of SiO_x and AlO_x domains.

Alternatively, hydrophilic aluminosilica moieties can be more readily introduced into the membrane framework by 'staged processing', which allows $(Al,Si)O_x$ species to be covalently grafted to interior pore surface sites. Such aluminosilica surface moieties can be effectively introduced under more suitable alkaline conditions, compared to the more acidic solution conditions from which the mesostructured silica films are cast. Post-synthesis modification of the siliceous mesopore walls provides an effective means of controlling both the amount and distribution of aluminosilica species incorporated, notably at surface sites that are accessible and can promote guest transport in the mesopore channels.

By adjusting the time and temperature to which mesoporous silica films are exposed to hydrolyzed alumina species in an alkaline $NaAlO_2$ solution, the amount of four-coordinated aluminum in the silica framework was controlled. Elemental analyses established that films with bulk molar ratios of Si/Al = 50 down to Si/Al = 5 could be obtained by controlling the reaction time from 1 to 12 h. Furthermore, quantitative single-pulse ^{27}Al MAS NMR spectra (Supporting Information Fig. S3) indicate that 90 % of the incorporated Al atoms are four-coordinated, consistent with aluminosilica species that are covalently bonded to the silica framework along the interior surfaces of the mesopore walls. For a mesostructured aluminosilica film with a bulk molar ratio Si/Al = 15, a mean surface coverage of 1.1 Al framework site nm^{-2} is established by elemental analyses and single-pulse ^{27}Al MAS NMR. As shown in Figure 2c, the long-range mesostructural ordering of the free-standing aluminosilica film (Si/Al = 15) remains intact and comparable to the solvent-extracted, free-standing mesoporous silica film (Fig. 2b).

The incorporation of four-coordinated aluminosilica sites along the interior pore walls of mesoporous silica increases the hydrophilicity of the free-standing films. This is demonstrated in Figure 3, which shows correlated thermogravimetric

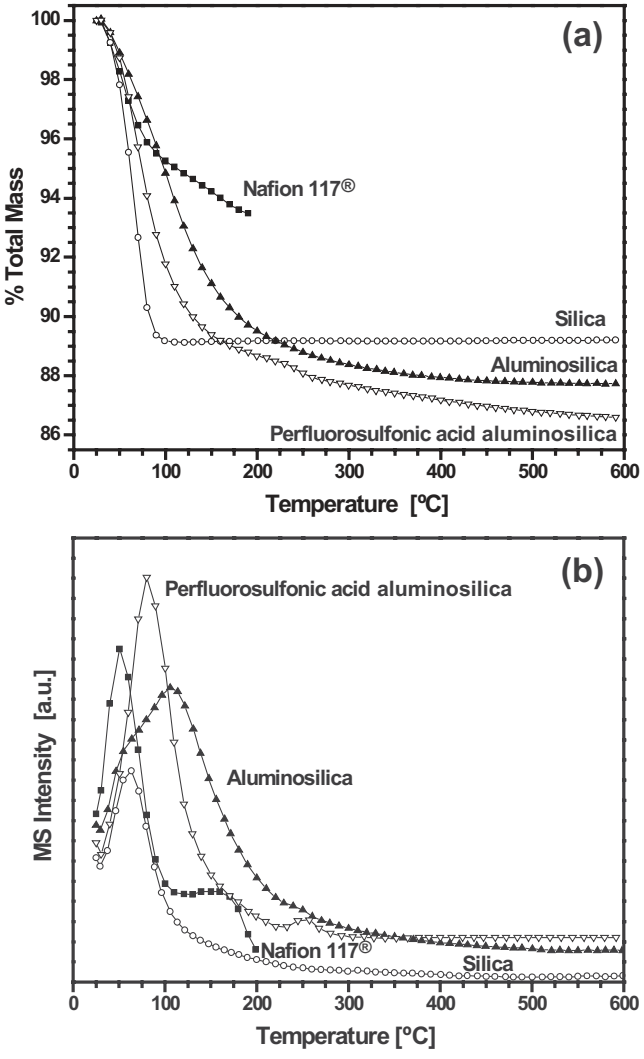

Figure 3. a) Thermogravimetric analyses (TGA) and b) correlated mass spectrometry traces of effluent gases from a solvent-extracted free-standing 62 μm-thick cubic mesoporous silica film [○], after aluminosilica surface grafting (1.1 Al site/nm^2) [▲], with both perfluorosulfonic-acid- and aluminosilica-surface-grafted species [▽], and from a Nafion 117® membrane [■]. By monitoring desorbing species with mass per charge $m/Z = 18$, the total mass loss measured in (a) was correlated specifically to desorbing water in (b), as functions of temperature. Incorporation of aluminosilica surface species onto the pore walls of the mesoporous silica films yields significantly higher adsorbed water capacity and water retention at temperatures above 100 °C, compared to mesoporous silica and Nafion 117®.

ADVANCED MATERIALS

analyses (TGA, Fig. 3a) and mass spectrometry measurements (Fig. 3b) associated with mass loss from the film as it is heated. By monitoring the effluent TGA gas stream using a mass spectrometer, mass loss as a function of temperature can be attributed to the desorption of specific species, in particular water. For example, a well-resolved mass spectrometry signal is obtained for desorbing species with a molecular weight of 18 g mol^{-1} over the range 0–600 °C from both the free-standing solvent-extracted mesoporous silica and aluminosilica-grafted films (Fig. 3b), so that their total mass loss (Fig. 3a) is attributed to desorbed water. Fully hydrated aluminosilica-grafted mesoporous silica contains ca. 12 wt % water, compared to 11 wt % for the mesoporous silica, and 6 wt % for a Nafion 117® membrane hydrated and measured under identical conditions. The increased hydration capacity results from the introduction of framework Al sites along the interior surfaces of the large (ca. 10 nm) mesopores.

More importantly, Figure 3b shows that, in addition to their higher hydration capacities compared to Nafion 117® or mesoporous silica films, the aluminosilica-grafted mesostructured films retain water to substantially higher temperatures. Under identical conditions, Nafion 117® shows a sharp maximum in the temperature-programmed mass spectrometry signal corresponding to desorption of water ($m/Z = 18$) at 55 °C, with the majority of the water lost by 100 °C. The small increase in the mass spectrometry curve between 130–170 °C is attributed to desorption of water molecules associated with sulfonic acid sites. The cubic mesostructured silica film shows similar water retention properties, with a somewhat broader maximum occurring at 65 °C and weak temperature-programmed-desorption (TPD) signal intensity above 100 °C. By comparison, the aluminosilica-grafted mesostructured film shows a broad TPD maximum near 110 °C, with notable signal intensity persisting to above 200 °C. The incorporation of grafted aluminosilica sites onto the interior surfaces of cubic mesoporous films significantly enhances their water-holding capacities and desorption temperatures, due to stronger adsorption of water associated with the hydrophilic channel surfaces.

To incorporate strong acid properties, the aluminosilica-grafted mesostructured films were functionalized with perfluorosulfonic-acid (PFSA) moieties to create proton conduction pathways through the 3D-cubic interconnected pores. It is well-known that the strong electron-withdrawing character of nearby fluorine atoms increases the acid strengths of the sulfonic acid groups, which serve as the primary proton-conducting moieties in Nafion® and other materials.[48] Here, the perfluorosulfonic-acid moieties were covalently bonded to the previously-aluminosilica-grafted pore surfaces through the reaction of cyclic 1,2,2-trifluoro-2-hydroxy-1-trifluoromethylethane-sulfonic-acid-*beta*-sultone with surface hydroxyl species on the mesopore walls.[48] Acid loadings of 2 wt % or 2.9 molecules nm^{-2} were achieved, with little effect on the overall mesostructural ordering of the film, as established by the SAXS pattern in Figure 2d. The perfluorosulfonic-acid moieties that result are covalently grafted to the silica framework via alkyl chains with electron-withdrawing fluorine atoms that impart strong acid properties to the material and also affect film hydrophilicity.

As shown in Figure 3a, TGA results show that the combined perfluorosulfonic-acid-aluminosilica mesostructured films have hydration capacities that are comparable to the aluminosilica-grafted films, up to ~12 wt % water. The relatively hydrophobic fluorinated alkyl chains, however, diminish somewhat the water-retention properties of the PFSA-aluminosilica-grafted films, with a maximum TPD mass spectrometry signal occurring at 85 °C and signal intensity indicating desorption of water persisting to 200 °C. These values are intermediate between those measured for Nafion 117® and the non-PFSA-containing aluminosilica materials. The TGA data, furthermore, show that the grafted perfluorosulfonic acid moieties are stable to 225 °C, above which they decompose. The TGA and mass spectrometry results establish that the total water content is nearly the same for the aluminosilica-grafted mesostructured silica films with and without the incorporated perfluorosulfonic-acid moieties.

The primary purpose of a proton-exchange membrane in a PEM fuel cell is to allow the protons produced at anodic catalytic sites to traverse selectively the membrane to the cathode, where they combine with adsorbed oxygen atoms to produce water. At higher temperatures for many PEM materials, dehydration effects lead to reduced proton mobilities and channel pinch-off that result in lower overall proton conductivities. For example, Figure 4 shows proton conductivities measured using AC impedance spectroscopy (see Experimental Sec.),[49] as functions of temperature for commercially available Nafion

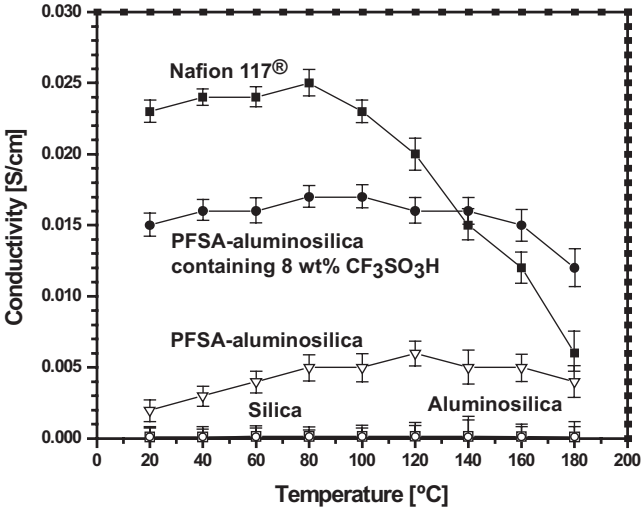

Figure 4. Conductivities measured as functions of temperature at 50 % relative humidity for Nafion 117® [■] and different 62 μm-thick films of mesoporous cubic SBA-16 silica functionalized sequentially as follows: solvent-extracted silica [<kl>], aluminosilica-grafted [□], perfluorosulfonic-acid- (PFSA) and aluminosilica-grafted [▽], and PFSA-aluminosilica-grafted and containing 8 wt % CF_3SO_3H (triflic acid) [°]. All films were initially hydrated with de-ionized water. The silica, aluminosilica, and perfluorosulfonic-acid aluminosilica films correspond to the same films measured in Figure 3.

117® and several differently functionalized, free-standing mesostructured silica films. All of the measurements were performed at 50 % relative humidity (R.H.) in an environmental chamber that allowed for control of humidity and temperature. Proton conductivities for Nafion 117® are shown for comparison: high values are obtained (ca. 2.4×10^{-2} S cm^{-1}) up to ca. 80 °C, but diminish considerably at higher temperatures, due to desorption of water from the membrane (Fig. 3b) and/or morphological changes in its structure at temperatures near the glass transition temperature of Nafion (~ 110 °C).[49a] The nascent SBA-16 cubic mesostructured silica film and the same film after aluminosilica-grafting exhibited low proton conductivities, $\sim 2 \times 10^{-5}$ S cm^{-1} and $\sim 1 \times 10^{-4}$ S cm^{-1}, respectively, over the temperature range of 20–180 °C. The former value for the purely siliceous film is in agreement with conductivities previously reported in literature.[40] The order-of-magnitude increase in the still-low proton conductivity of the aluminosilica-grafted film is attributed to the presence of acid sites introduced following incorporation of aluminosilica species onto the interior mesopore channel walls.

Upon grafting perfluorosulfonic-acid species onto the interior mesopore surfaces of the cubic SBA-16 mesostructured aluminosilica film, the proton conductivity values increased by another order of magnitude. As shown in Figure 4, *co*-PFSA-aluminosilica-functionalized mesoporous silica yields conductivities of ca. 5×10^{-3} S cm^{-1}, increasing moderately with temperature to approximately 120 °C and maintaining stable values thereafter up to 180 °C. Still higher proton conductivities are obtained if the remaining mesopore volumes are filled with strong acid species, such as for example CF_3SO_3H (triflic) acid, instead of water or a non-conducting barrier component (to reduce solvent cross-over.) Such acid species can be introduced by solution imbibition into the previously perfluorosulfonic-acid- and aluminosilica-grafted mesopore channels, thereby increasing still further the concentration of proton conducting moieties in the films. For the case of co-functionalized PFSA-aluminosilica films back-filled with 8 wt % triflic acid, proton conductivities up to 1.7×10^{-2} S cm^{-1} are obtained at 50 % R.H., close to that of Nafion 117® (2.4×10^{-2} S cm^{-1}.) In addition, the conductivity values of the functionalized films are notably stable, remaining above 1.5×10^{-2} S cm^{-1} to 160 °C and surpassing values measured under identical conditions for Nafion 117® above 135 °C. This is due to the improved water retention properties and stable conducting channels provided by the perfluorosulfonic-acid- and aluminosilica-grafted cubic mesostructured films. At full saturation conditions (100 % R.H.), bothe the co-functionalized PFSA-aluminosilica films back-filled with 8 wt % triflic acid and Nafion 117® membranes show improved conductivity values (Supporting Information Fig. S4) that are stable over the temperature range 120–160 °C.

Proton conductivities in the co-functionalized PFSA-aluminosilica-grafted films were examined as functions of triflic acid concentration, with maximum conductivity values measured for films containing 8 wt % triflic acid (Fig. 4). Similar conductivity maxima have been observed for homogeneous acid solutions and attributed to the beneficial effects of higher acid concentrations being offset by reduced local hydration effects[7] or increased viscous resistance to proton transport.[50] While the triflic acid species appear to be stably incorporated within the mesopore channels, enhanced stability and solvent-barrier properties are anticipated for grafted or larger molecular weight acidic filler species. The combination of enhanced hydrophilicity, robust mesostructured channels, and strong acid functionality imparts superior high temperature (> 135 °C) proton conductivity properties to PFSA-aluminosilica-functionalized mesostructured silica films, compared to Nafion 117®.

In summary, the benefits of staged-processing allow the separate optimization of conditions needed to achieve high extents of cubic mesostructural ordering, 3D pore interconnectivities, functionalization, and macroscopic film processability without cracks, required for optimizing membrane transport properties. Free-standing and thin-film mesostructured silica films containing 3D interconnected pore networks were synthesized and their interior pore surfaces functionalized with aluminosilica and perfluorosulfonic-acid species to create highly interconnected hydrophilic pathways across the thickness of the films through which proton conduction can occur. Treatment of the perfluorosulfonic-acid- and aluminosilica-grafted mesostructured films with triflic acid yielded both high water retention and higher proton conductivity values, which exceeded those of Nafion 117® at temperatures above 135 °C. These novel acid-functionalized, mesostructured aluminosilica films provide a promising alternative to currently used perfluorosulfonic-acid polymeric materials in proton-exchange membrane fuel cells operating at temperatures above 150 °C.

Experimental

Mesostructured silica films possessing body-centered-cubic $Im\bar{3}m$ ordering were prepared, as described previously: [44,45] 2.0 g of the poly(ethylene oxide)-poly(propylene oxide)-poly(ethylene oxide) triblock copolymer Pluronic F127 ($EO_{106}PO_{70}EO_{106}$) from BASF were dissolved in 20 g C_2H_5OH, and separately, a silica sol solution was prepared consisting of 8.2 g tetraethoxysilane (TEOS), 0.007 g HCl, 3.6 g water, and 12 g C_2H_5OH. The separate solutions were covered, stirred at room temperature for 1 h, and then mixed to yield a precursor solution with a molar ratio of 1.0 TEOS: 0.004 F127: 0.0045 HCl: 5.0 H_2O: 20 C_2H_5OH, which was subsequently stirred for an additional 2 h at room temperature. Supported thin films were formed by dip-coating, in which a polished silicon substrate was removed vertically from the precursor solution at a rate of ~ 3 mm s^{-1}. Free-standing films were formed by casting the precursor solution in a loosely covered polystyrene Petri dish and allowing the volatile solvents to evaporate under ambient conditions over approximately 1 week. For the supported silica films, the structure-directing triblock copolymer species were removed and silica cross-linking increased by thermal oxidation (calcination) in air. This was achieved by heating the films at 1 °C min^{-1} to 550 °C and holding at this temperature for 8 h to produce smooth crack-free thin films. The triblock copolymer species in the free-standing films were solvent extracted by refluxing in ethanol for 24 h to minimize thermally induced micro-cracking. Solvent ex-

ADVANCED MATERIALS

traction effectively removed 95 % of the triblock copolymer species from the free-standing films.

Aluminosilica species were formed at silica surface sites in the mesopores by covalently grafting hydrolyzed alumina species under alkaline solution conditions using a procedure similar to that described previously [46]. 1.0 g of the free-standing mesoporous silica films was placed in a polypropylene bottle containing 50 mL of 0.25 M $NaAlO_2$ in de-ionized water, and the sealed bottled was heated and held at 60 °C under gentle stirring for 12 h. The supported silica thin films were kept at room temperature, instead of 60 °C, for the 12 h grafting reaction, under otherwise identical conditions. The resulting aluminosilica-grafted mesostructured films were washed with de-ionized water. Remaining sodium cations in the films were removed by ion-exchange by soaking the films in 1.0 M H_2SO_4 (aq.) for 1 h, followed by rinsing in de-ionized water. This ion-exchange process was repeated three times to remove over 90 % of the sodium in the sample, as determined by solid-state ^{23}Na NMR.

Perfluorosulfonic-acid moieties were grafted onto the aluminosilica mesopore surfaces of the films using the procedure reported by Alvaro and co-workers [48]. The ion-exchanged, aluminosilica-grafted films were first dried under vacuum at 120 °C overnight, then 2.0 g of the dried aluminosilica-grafted films were placed in a solution containing 1.0 g of 1,2,2-trifluoro-2-hydroxy-1-trifluoromethylethane-sulfonic-acid-*beta*-sultone in 50 mL of dry toluene under an inert atmosphere. The reaction mixture was refluxed for 4 h, washed in toluene, and finally dried at 100 °C in air. For the film containing 8 wt % triflic acid, the PFSA-functionalized aluminosilica sample was soaked in 4 M aqueous CF_3SO_3H (triflic acid) at room temperature for 10 min and then prepared as described below prior to the conductivity measurements.

SEM images were collected using an FEI XL40 Sirion microscope with an accelerating voltage of 3 kV on films coated with gold/palladium. TEM samples were prepared by removing the mesostructured supported films from the substrates by using a razor blade or grinding the free-standing films into powders, forming slurries of the powders in ethanol, and dispersing them on a holey carbon grid. TEM images were collected on a JEOL 2010 microscope operating at 200 kV. 2D small-angle X-ray scattering (SAXS) patterns were collected using 1.54 Å Cu Kα radiation generated by a fine-focus (0.2 mm) Rigaku rotating-angle generator and detected on a Bruker HI-STAR multiwire area detector. The free-standing silica films were positioned in the sample holder in transmission mode. 1D diffraction patterns were obtained from the 2D scattering data by 2θ integration using the computer program Fit2D [51]. Thermogravimetric analyses, combined with mass spectroscopy, of the effluent gases were performed on a Mettler TGA/sDTA851e ThermoGravimetric Analyzer coupled to a Blazers ThermoStar Mass Spectrometer. Samples were heated from 25 °C to 600 °C at a rate of 10 °C min^{-1} under constant nitrogen gas flow of 25 L min^{-1}.

Proton conductivities were measured by using a Solartron 1260 Impedance/Gain-Phase Analyzer over the frequency range 0.1 Hz to 1 MHz with an AC amplitude of 10 mV. The samples, except for the triflic-acid containing films, were soaked in either de-ionized water and all samples were allowed to dry overnight in air at 50 °C prior to measurement. Each sample was placed in a Teflon® measurement cell similar to that described by Zawodzinski and co-workers [49], and electrical contacts were established by using platinum foil electrodes. The measurement cell containing the sample was placed in a stainless-steel chamber along with a known quantity of de-ionized water that depended upon the mass required to yield a relative humidity (R.H.) of 50 % at each temperature. Prior to measuring the conductivity, dry nitrogen was passed through the chamber for 2 min, after which the chamber was closed and then heated to the desired temperature. After 2 h, during which time the temperature in the closed chamber stabilized and the de-ionized water evaporated to yield an atmosphere of 50 % R.H. (1–3 atm), the conductivity measurements were performed. Nyquist impedance plots were generated using the ZPlot/ZView software package, and the ohmic resistance of each film was taken to be the real impedance value when the imaginary impedance approached zero at the low frequency intercept.

Received: December 5, 2006
Revised: March 8, 2007
Published online: August 9, 2007

[1] H.-F. Oetjen, V. M. Schmidt, U. Stimming, F. Trila, *J. Electrochem. Soc.* **1996**, *143*, 3838.
[2] Q. Li, R. He, J.-A. Gao, J. O. Jensen, N. J. Bjerrum, *J. Electrochem. Soc.* **2003**, *150*, A1599.
[3] R. Jiang, H. R. Kunz, J. M. Fenton, *J. Electrochem. Soc.* **2005**, *152*, A1329.
[4] R. K. A. M. Mallant, *J. Power Sources* **2003**, *118*, 424.
[5] P. Costamagna, S. Srinivasan, *J. Power Sources* **2001**, *102*, 253.
[6] Z. Liu, J. S. Wainright, R. F. Savinell, *Chem. Eng. Sci.* **2004**, *59*, 4833.
[7] V. S. Murthi, R. C. Urian, S. Mukerjee, *J. Phys. Chem. B* **2004**, *108*, 11 011.
[8] R. Farrauto, S. Hwang, L. Shore, W. Ruettinger, J. Lampert, T. Giroux, Y. Liu, O. Ilinich, *Annu. Rev. Mater. Res.* **2003**, *33*, 1.
[9] C. Yang, P. Costamagna, S. Srinivasan, J. Benziger, A. B. Bocarsly, *J. Power Sources* **2001**, *103*, 1.
[10] R. F. Silva, M. De Francesco, A. Pozio, *J. Power Sources* **2004**, *134*, 18.
[11] T. A. Zawodzinski, Jr., T. E. Springer, F. Uribe, S. Gottesfeld, *Solid State Ionics* **1993**, *60*, 199.
[12] K. D. Kreuer, *Solid State Ionics* **1997**, *97*, 1.
[13] A. V. Anantaraman, C. L. Gardner, *J. Electroanal. Chem.* **1996**, *414*, 115.
[14] T. A. Zawodzinski, Jr., C. Derouin, S. Radzinski, R. J. Sherman, V. T. Smith, T. E. Springer, S. Gottesfeld, *J. Electrochem. Soc.* **1993**, *140*, 1041.
[15] J.-M. Bae, I. Honma, M. Murata, T. Yamamoto, M. Rikukawa, N. Ogata, *Solid State Ionics* **2002**, *147*, 189.
[16] D. I. Ostrovskii, L. M. Torell, M. Paronen, S. Hietala, F. Sundholm, *Solid State Ionics* **1997**, *97*, 315.
[17] R. W. Kopitzke, C. A. Linkous, H. R. Anderson, G. L. Nelson, *J. Electrochem. Soc.* **2000**, *147*, 1677.
[18] F. Wang, M. Hickner, Y. S. Kim, T. A. Zawodzinski, J. E. McGrath, *J. Membr. Sci.* **2002**, *197*, 231.
[19] R. He, Q. Li, G. Xiao, N. J. Bjerrum, *J. Membr. Sci.* **2003**, *226*, 169.
[20] H. Pu, W. H. Meyer, G. Wegner, *J. Polym. Sci. Part B* **2002**, *40*, 663.
[21] B. Bonnet, D. J. Rozière, L. Tchicaya, G. Alberti, M. Casciola, L. Massinelli, B. Bauer, A. Peraio, E. Ramunni, *J. New Mater. Electrochem. Syst.* **2000**, *3*, 87.
[22] K. T. Adjemian, S. J. Lee, S. Srinivasan, J. Benziger, A. B. Bocarsly, *J. Electrochem. Soc.* **2002**, *149*, A256.
[23] Q. Li, R. He, J. O. Jensen, N. J. Bjerrum, *Chem. Mater.* **2003**, *15*, 4896.
[24] P. Jannasch, *Curr. Opin. Colloid Interface Sci.* **2003**, *8*, 96.
[25] L. Qingfeng, H. A. Hjuler, N. J. Bjerrum, *J. Appl. Electrochem.* **2001**, *31*, 773–779.
[26] K. A. Mauritz, I. D. Stefanithis, S. V. Davis, R. W. Scheetz, R. K. Pope, G. L. Wilkes, H. Huang, *J. Appl. Polym. Sci.* **1995**, *55*, 181.
[27] P. L. Antonucci, A. S. Aricò, P. Cretì, E. Ramunni, V. Antonucci, *Solid State Ionics* **1999**, *125*, 431.
[28] H. Uchida, Y. Ueno, H. Hagihara, M. Watanabe, *J. Electrochem. Soc.* **2003**, *150*, A57.
[29] B. A. Holmberg, S.-J. Hwang, M. E. Davis, Y. Yan, *Microporous Mesoporous Mater.* **2005**, *80*, 347.
[30] S. Hamoudi, S. Royer, S. Kaliaguine, *Microporous Mesoporous Mater.* **2004**, *71*, 17.
[31] M. I. Ahmad, S. M. J. Zaidi, S. U. Rahman, S. Ahmed, *Microporous Mesoporous Mater.* **2006**, *91*, 296.

[32] H. Wang, B. A. Holmberg, L. Huang, Z. Wang, A. Mitra, J. M. Norbeck, Y. Yan, *J. Mater. Chem.* **2002**, *12*, 834.
[33] Z. Chen, B. Holmberg, W. Li, X. Wang, W. Deng, R. Munoz, Y. Yan, *Chem. Mater.* **2006**, *18*, 5669.
[34] D. Coutinho, Z. Yang, J. P. Ferraris, K. J. Balkus, Jr., *Microporous Mesoporous Mater.* **2005**, *81*, 321.
[35] B. Smitha, S. Sridhar, A. A. Khan, *J. Membr. Sci.* **2005**, *259*, 10.
[36] W. H. J. Hogarth, J. C. Diniz da Costa, G. Q. Lu, *J. Power Sources* **2005**, *142*, 223.
[37] J. Weitkamp, *Solid State Ionics* **2000**, *131*, 175.
[38] J. J. Chiu, D. J. Pine, S. T. Bishop, B. F. Chmelka, *J. Catal.* **2004**, *221*, 400.
[39] M. T. Janicke, C. C. Landry, S. C. Christiansen, D. Kumar, G. D. Stucky, B. F. Chmelka, *J. Am. Chem. Soc.* **1998**, *120*, 6940.
[40] H. Li, M. Nogami, *Adv. Mater.* **2002**, *14*, 912.
[41] H. Yang, A. Kuperman, N. Coombs, S. Mamiche-Afara, G. A. Ozin, *Nature* **1996**, *379*, 703.
[42] C. J. Brinker, Y. Lu, A. Sellinger, H. Fan, *Adv. Mater.* **1999**, *11*, 579.
[43] D. Grosso, F. Cagnol, G. J. de A. A. Soler-Illia, E. L. Crepaldi, H. Amenitsch, A. Brunet-Bruneau, A. Bourgeois, C. Sanchez, *Adv. Funct. Mater.* **2004**, *14*, 309.
[44] D. Zhao, P. Yang, N. Melosh, J. Feng, B. F. Chmelka, G. D. Stucky, *Adv. Mater.* **1998**, *10*, 1380.
[45] P. C. A. Alberius, K. L. Frindell, R. C. Hayward, E. J. Kramer, G. D. Stucky, B. F. Chmelka, *Chem. Mater.* **2002**, *14*, 3284.
[46] Z. Luan, M. Hartmann, D. Zhao, W. Zhou, L. Kevan, *Chem. Mater.* **1999**, *11*, 1621.
[47] D. R. Dunphy, S. Singer, A. W. Cook, B. Smarsly, D. A. Doshi, C. J. Brinker, *Langmuir* **2003**, *19*, 10 403.
[48] a) M. Alvaro, A. Corma, D. Das, V. Fornés, H. García, *Chem. Commun.* **2004**, 956. b) M. Alvaro, A. Corma, D. Das, V. Fornés, H. García, *J. Catal.* **2005**, *231*, 48.
[49] a) M. Casciola, G. Alberti, M. Sganappa, R. Narducci, *J. Power Sources* **2006**, *162*, 141. b) T. A. Zawodzinski, Jr., M. Neeman, L. O. Sillerud, S. Gottesfeld, *J. Phys. Chem.* **1991**, *95*, 6040.
[50] D.-T. Chin, H. H. Chang, *J. Appl. Electrochem.* **1989**, *19*, 95.
[51] A. P. Hammersley, *ESRF Internal Report*, ESRF97HA02T, **1997**.
[52] G. L. Athens, *Ph.D. Thesis*, University of California, Santa Barbara **2007**.

